Since January 2020 Elsevier has created a COVID-19 resource centre with free information in English and Mandarin on the novel coronavirus COVID-19. The COVID-19 resource centre is hosted on Elsevier Connect, the company's public news and information website.

Journal of Hazardous Materials 397 (2020) 122609

Contents lists available at ScienceDirect

Journal of Hazardous Materials

journal homepage: www.elsevier.com/locate/jhazmat

Transmission of pathogen-laden expiratory droplets in a coach bus

Xia Yang[a], Cuiyun Ou[a], Hongyu Yang[a], Li Liu[b], Tie Song[c], Min Kang[c], Hualiang Lin[d], Jian Hang[a,e,*]

[a] School of Atmospheric Sciences, Guangdong Province Key Laboratory for Climate Change and Natural Disaster Studies, Sun Yat-sen University, Guangzhou, PR China
[b] Department of Building Science, School of Architecture, Tsinghua University, Beijing, 100084, PR China
[c] Guangdong Provincial Center for Disease Control and Prevention, Guangzhou, PR China
[d] Department of Epidemiology, School of Public Health, Sun Yat-sen University Guangzhou, PR China
[e] Southern Marine Science and Engineering Guangdong Laboratory (Zhuhai), Zhuhai, PR China

GRAPHICAL ABSTRACT

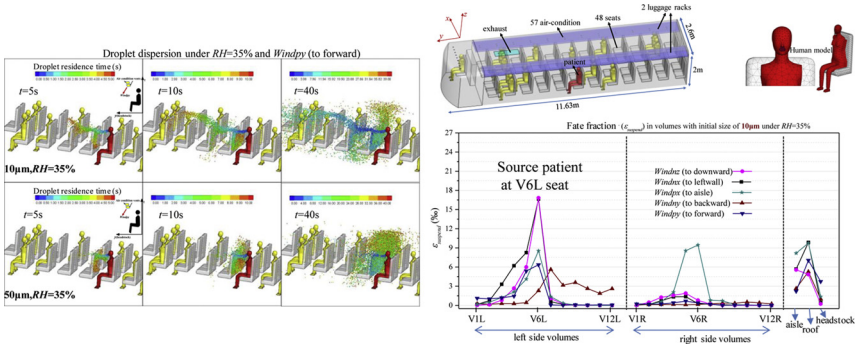

ARTICLE INFO

Editor: D. Aga

Keywords:
Droplet dispersion
Droplet evaporation
Enclosed bus environment
Computational fluid dynamic (CFD) simulation
Relative humidity

ABSTRACT

Droplet dispersion carrying viruses/bacteria in enclosed/crowded buses may induce transmissions of respiratory infectious diseases, but the influencing mechanisms have been rarely investigated. By conducting high-resolution CFD simulations, this paper investigates the evaporation and transport of solid-liquid mixed droplets (initial diameter 10 μm and 50 μm, solid to liquid ratio is 1:9) exhaled in a coach bus with 14 thermal manikins. Five air-conditioning supply directions and ambient relative humidity (*RH* = 35 % and 95 %) are considered.

Results show that ventilation effectiveness, *RH* and initial droplet size significantly influence droplet transmissions in coach bus. 50 μm droplets tend to evaporate completely within 1.8 s and 7 s as *RH* = 35 % and 95 % respectively, while 0.2 s or less for 10 μm droplets. Thus 10 μm droplets diffuse farther with wider range than 50 μm droplets which tend to deposit more on surfaces. Droplet dispersion pattern differs due to various interactions of gravity, ventilation flows and the upward thermal body plume. The fractions of droplets suspended in air, deposited on wall surfaces are quantified. This study implies high *RH*, backward supply direction and passengers sitting at nonadjacent seats can effectively reduce infection risk of droplet transmission in buses. Besides taking masks, regular cleaning is also recommended since 85 %–100 % of droplets deposit on object surfaces.

* Corresponding author.
E-mail address: hangj3@mail.sysu.edu.cn (J. Hang).

https://doi.org/10.1016/j.jhazmat.2020.122609
Received 15 February 2020; Received in revised form 25 March 2020; Accepted 27 March 2020
Available online 12 April 2020

1. Introduction

Respiratory infectious diseases, such as tuberculosis (TB), influenza, Middle East Respiratory Syndrome (MERS) and severe acute respiratory syndrome (SARS) have threatened public health in the last twenty years (World Health Organization, 2020a). Recently, the novel coronavirus (SARS-CoV-2) which is rampant in China and even throughout the world has a strong ability of human to human infection, which attracts the attention of WHO (World Health Organization, 2020b). In various indoor environments, it is well known that the solid-liquid mixed droplets exhaled by different respiratory activities (breathing, talking, coughing and sneezing, etc.) may carry infectious bacteria or viruses which evaporate, spread, suspend in air or trapped at wall surfaces, and then can be inhaled or exposed to human body and hence produce potential infection risk (Yu et al., 2004; Zhou et al., 2018; Bartzis et al., 2015).

With the acceleration of urbanization process, the demands on intercity and suburban traffic grow continually. Especially in China, the coach bus is popular because of its high speed, comfort and convenience. For instance, a large number of migrant workers return home with long-distance buses which are overcrowded during every Chinese Spring Festival. Furthermore, the coach bus is an enclosed and crowded indoor space where many passengers stay for several hours and the air mainly circulates inside the bus, which may raise the risk of droplet transmissions of infectious diseases. Recently, the infection cases of novel coronavirus in bus environment have been found in China. 11 passengers were confirmed infected after taking the same vehicles with a novel coronavirus patient. According to the survey, the infected passenger who seat 4.5 m far away from the patient did not have close contact with patient on the whole trip. Thus the infection can be identified as airborne transmission. We performed tracer gas field measurements in that bus in April 2020 and will introduce this research in recent future.

Since the outbreak of SARS in 2003, there have been an abundance of experimental and/or numerical studies on indoor ventilation and airborne transmission in inter-units of buildings (Yu et al., 2004; Liu et al., 2011a, b), hospital isolation rooms (Li et al., 2007; Saravia et al., 2007; Kao and Yang, 2006; Lai and Cheng, 2007; Shih et al., 2007; Qian et al., 2006; Tung et al., 2009; Qian and Li, 2010; Hang et al., 2014; Sung et al., 2018) or operating rooms (Wang et al., 2018), general indoor environments (Cao et al., 2015; Wei et al., 2018). Besides for vehicle indoor environments, a number of studies emphasized indoor transmission in airplane cabins (Mazumdar et al., 2011; Han et al., 2014; Gupta et al., 2012; Yan et al., 2009) and high-speed train (Zhang and Li, 2012). For instance, Zhang and Li (2012) used CFD (Computational Fluid Dynamics) simulations to study the respiratory particle dispersion process (without droplet evaporation) in four different boundary conditions of air supply and exhausts in a high-speed rail cabin. However, there is a lack of study on ventilation and droplet dispersion in the coach bus.

Respiratory infectious diseases can be transmitted via three routes, namely contact, airborne and fomite (Castle and Wiley, 1987). Similarly, a higher risk of infection is associated with close proximity to the source patient and decrease rapidly with the distance (Kowalski and Bahnfleth, 1998; Lidwell and Williams, 1961; Wong et al., 2004; Mui et al., 2009; Lai et al., 2012; McGrath et al., 2019). With the same initial concentration, a larger quantity of mass released may be expected to experience a slower dilution (Scargiali et al., 2011; Pereira and Chen, 1996). Due to the initial velocity, the exhaled gas and particles can travel in the air over a distance which is determined by the ventilation airflow, gravity force related to particle diameters and buoyancy forces of thermal bodies (Qian and Li, 2010; Hang et al., 2014; Zhang and Li, 2012; Mui et al., 2009; McGrath et al., 2019; Gupta et al., 2010; Xu et al., 2015; Chao et al., 2009). Larger particles (> 50 μm) may settle on wall surfaces or floors quickly because the significance of gravity is greater than ventilation. Smaller particles ($0.5-10$ μm) may remain suspended for a sufficient time and lead to disease transmission over larger range (Qian and Li, 2010; Han et al., 2014; Zhang and Li, 2012; Chen and Zhao, 2010).

Apart from the initial droplet size, the droplet evaporation and dispersion may be influenced by the relative humidity (*RH*) in ambient environment as well (Ji et al., 2018). Wei and Li (2015) discovered that droplet dispersion with the diameter of 50 μm was very sensitive to *RH* in the jet-like cough airflow. By calculating the droplet lifetimes and droplet size variation with different *RH*, Xie et al. (2007) indicated that the droplet size was dictated by its evaporation and droplets smaller than 100 μm would evaporate before falling to the ground 2 m away. The shrinking aerosols would ultimately form droplet nuclei small enough to suspend in the air for substantial time. Accordingly, instead of using pure water droplets for model testing (Xie et al., 2007), test droplets containing nonvolatile content were investigated by Liu et al. (2017) and employed in our study too, which would ultimately form droplet nuclei after evaporation. Due to the great impact of initial droplet size on disease transmission, many studies were carried out to reveal the size profile information of droplets during different expiratory activities (Chao et al., 2009; Xie et al., 2009; Yang et al., 2007). It is difficult to identify the actual droplet size exhaled from different patients with various human activities. Therefore, we first emphasize and adopt the initial droplet diameters of 10 μm and 50 μm as involved in most previous studies.

In summary, there are many studies on the diffusion of tracer gases and particulate matter for indoor transmission in hospital ward, airplane cabin and general indoor environment etc. However, it is still a lack of studies on droplet evaporation and dispersion in enclosed bus environments.

This paper aims to investigate the effect of *RH* and indoor airflow pattern with body thermal plume on the evaporation and dispersion of exhaled droplets with different initial diameters in enclosed bus environment. The enclosed bus model followed the realistic coach bus that went from Guangzhou to Huizhou in Guangdong province P.R. China and carried a Korean patient infected by MERS (Middle East Respiratory Syndrome) in May 2015, who did not wear a mask and did not give a cough/sneeze or talk with others either. The other thirteen people were isolated for three weeks after this trip and fortunately no one was infected by this source patient. By cooperating with CDC of Guangdong province, we adopted the same passenger locations and average ventilation flow rates in the enclosed bus taken by MERS patient in CFD model settings. Then the impacts of *RH*, initial droplet diameters and air-conditioning supply directions can be investigated as case studies by CFD simulations. Through statistics of the number of droplets trapped, suspended and escaped to predict the chance of infection, this study attempts to provide some recommendations for reducing the risk of droplet transmissions in enclosed bus environments.

2. Methodology

2.1. Validation of numerical simulations

In this study, Ansys FLUENT (ANSYS Inc, 2020) was applied in the validation and following numerical cases study. As displayed in Fig. 1a, based on the experimental data of Yin et al. (2009) in an inpatient ward furnished with one patient, one visitor, one bed, a TV set and a piece of medical equipment, CFD validation study was first conducted to verify the ability of CFD in predicting indoor airflow and temperature distribution. According to the experiment (Yin et al., 2009), air was supplied from a near-floor diffuser with the temperature of 19.5℃ and ventilation rate of 4 ACH (114CFM), and air was exhausted through the bathroom exhaust and main exhaust with the ventilation rate of 36CFM and 78CFM respectively. The heat generated by patient, visitor, equipment and TV was 106 W, 110 W, 36 W and 24 W. More details can be found in Yin et al. (2009). In our CFD simulations, the mesh was generated with the maximum grid size of 5 cm (fine grid, total

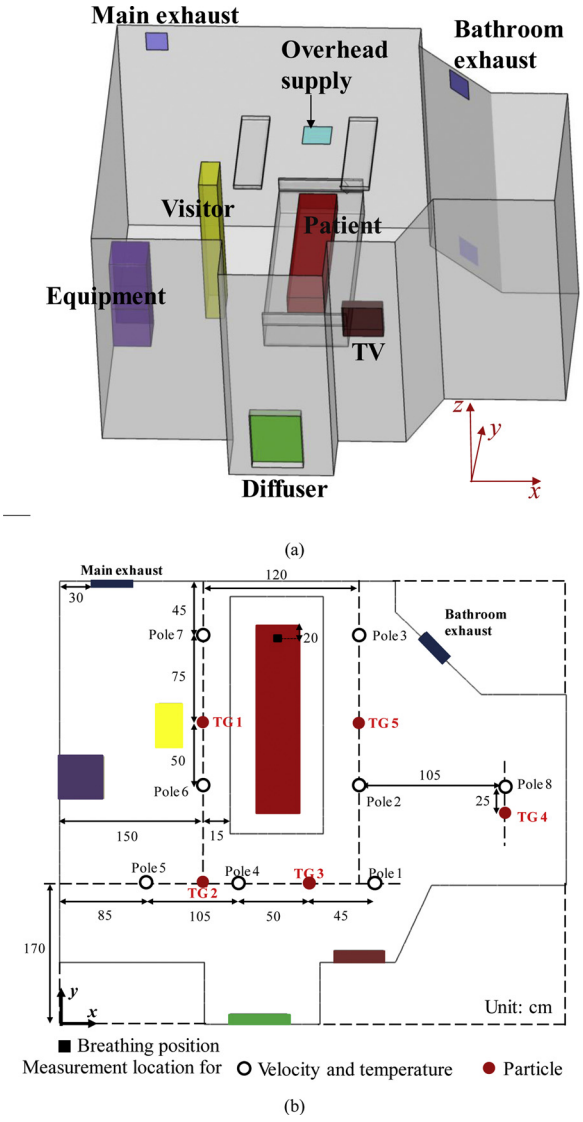

Fig. 1. Description of one-bed isolation room in CFD validation case referring to Yin et al. (2009).

tetrahedral cells of 1.8 million) and 10 cm (coarse grid, total tetrahedral cells of 0.38 million) near wall surfaces and finer grids near heating surfaces.

As shown in Fig. 1b, vertical profiles of velocity magnitude and static temperature were measured at seven heights of 0.12 m, 0.35 m, 0.85 m, 1.35 m, 1.86 m, 2.35 m and 2.6 m from the floor in 8 poles. The particle concentrations were measured in 5 poles, namely TG1-TG5 at six heights of 0.12 m, 0.60 m, 1.1 m, 1.6 m, 2.1 m and 2.6 m. These experimental results were used to evaluate the accuracy of CFD simulation for contrast. As an example, Fig. 2 depicts the vertical profiles of normalized velocity (u/u_s, u_s is the supply air velocity equals to 0.14 m/s) and temperature ($\Theta=(T\text{-}T_s)/(T_e\text{-}T_s)$, T_s and T_e are the temperature respectively at inlet and main exhaust) in the normalized height (z/H, H is the height of the inpatient ward equals to 2.7 m) from both experimental data and numerical results at Pole 1, Pole 2. The comparison indicates that the CFD simulation slightly underestimates the velocity and temperature values. The fine grid performs as well as the coarse grid in Θ prediction (Fig. 2b, d). While the fine grid arrangements can better predict the trend of U (Fig. 2a). Therefore, fine grid arrangement is utilized in our later case investigations. The deviation between the fine grid simulation results and experimental data is quantified by means of computing fractional bias (FB) which can give the information about overestimation or underestimation. The FB values indicate that simulation results of Θ and U generally underestimate (i.e. -0.04 to -0.23).

After the steady-state airflow being solved, particles with diameter of 1 μm were released from the patient mouth into the ward with a constantly negligible releasing velocity. The experimental data and numerical results of particle concentration profiles are shown in Fig. 2e–h. Figures reveal that, for TG5 which close to the contaminant source and the exhaust where the airflow was unstable, both the particle concentration measured in experiment and CFD display a large fluctuation. The particle concentration on TG1, TG3, TG4 is relatively small and has similar profile shape. The results show not very good simulation of concentration values but sufficiently well in predicting the changing shape and magnitude of particle concentration. On the whole, the above results prove that present CFD simulations with RNG k-ε model and grid arrangement with the maximum grid size of 5 cm is effective (Hang et al., 2014; Mazumdar et al., 2011; Zhang and Li, 2012; Hang et al., 2015) and can be adopted in the following simulation of indoor environments.

2.2. Model description and numerical case design

This study aims to figure out the characteristics of droplet evaporation and dispersion in an enclosed long-route coach bus. A realistic coach bus, with a dimension of 11.63 m × 2.6 m × 2 m ($L\times W\times H$), was adopted to investigate the influence of air-conditioning supply directions and indoor relative humidity. The detailed descriptions of enclosed bus are summarized in Table 1 and Fig. 3. Following the data from CDC of Guangdong province, 14 thermal manikins including 13 passengers (i.e. one infected and 12 healthy passengers) and a driver, were positioned at different seats in the bus model. All seats were numbered as shown in Fig. 3b. The infected passenger was located at Seat 6A. Two air-conditioning supplies with a dimension of 0.04 m × 0.03 m ($L\times W$) were respectively located near the two-side walls on the lower level of luggage carriers. Nine vents were arranged on the ceiling at the headstock. The exhaust was located on the ceiling near the second row of bus and its dimension was 1.185 m × 0.36 m ($L\times W$) (Fig. 4). We divided the bus model into 27 zones as shown in Fig. 3, including headstock, aisle, roof and the other 24 zones separated by the seats.

We used Gambit to build the bus model and the inside, and generate the unstructured mesh. Refined boundary layers were employed near mouths, noses, exhaust, and air-conditioning vents where the velocity gradient may be larger (Fig. 5). The mesh sizes of the mouth and nose are set as 0.005 m, which are smaller than 0.05 m around the human body. Similarly, the mesh sizes on the exhaust and air-conditioning vents are 0.01 m. While for the bodywork, the sizes are 0.05 m. The number of total grid elements was about 2, 790, 000, which was determined by refining the mesh until the flow field solution was grid-independent. Zhao et al. (2004) found that the dispersion of exhaled particles was easily affected by the size of particles, body thermal plumes and ventilation airflow patterns. So we investigated the particle dispersion and deposition in terms of various initial sizes of droplets, air condition supply directions and RH.

Table 2 lists the simulation cases. 10 μm and 50 μm droplets were used to respectively show the distinct dispersion characteristics for small and big droplets. The characteristics for droplet dispersion were related to not only their sizes but also the indoor airflow features. In real cases, passengers may change the air supply direction for personalized temperature or wind speed. To simplify our simulation, we assumed that the air supply directions were similar for all air-conditioning vents. Thus, a series of cases referring to different air-conditioning supply modes were employed including *Windnz* (to downward), *Windnx* (to the left wall), *Windpx* (to the aisle), *Windny* (to backward), and *Windpy* (to forward) (Fig. 5a, b). Environmental relative humidity (RH) was set as 35 % and 95 %. Flow fields in surface

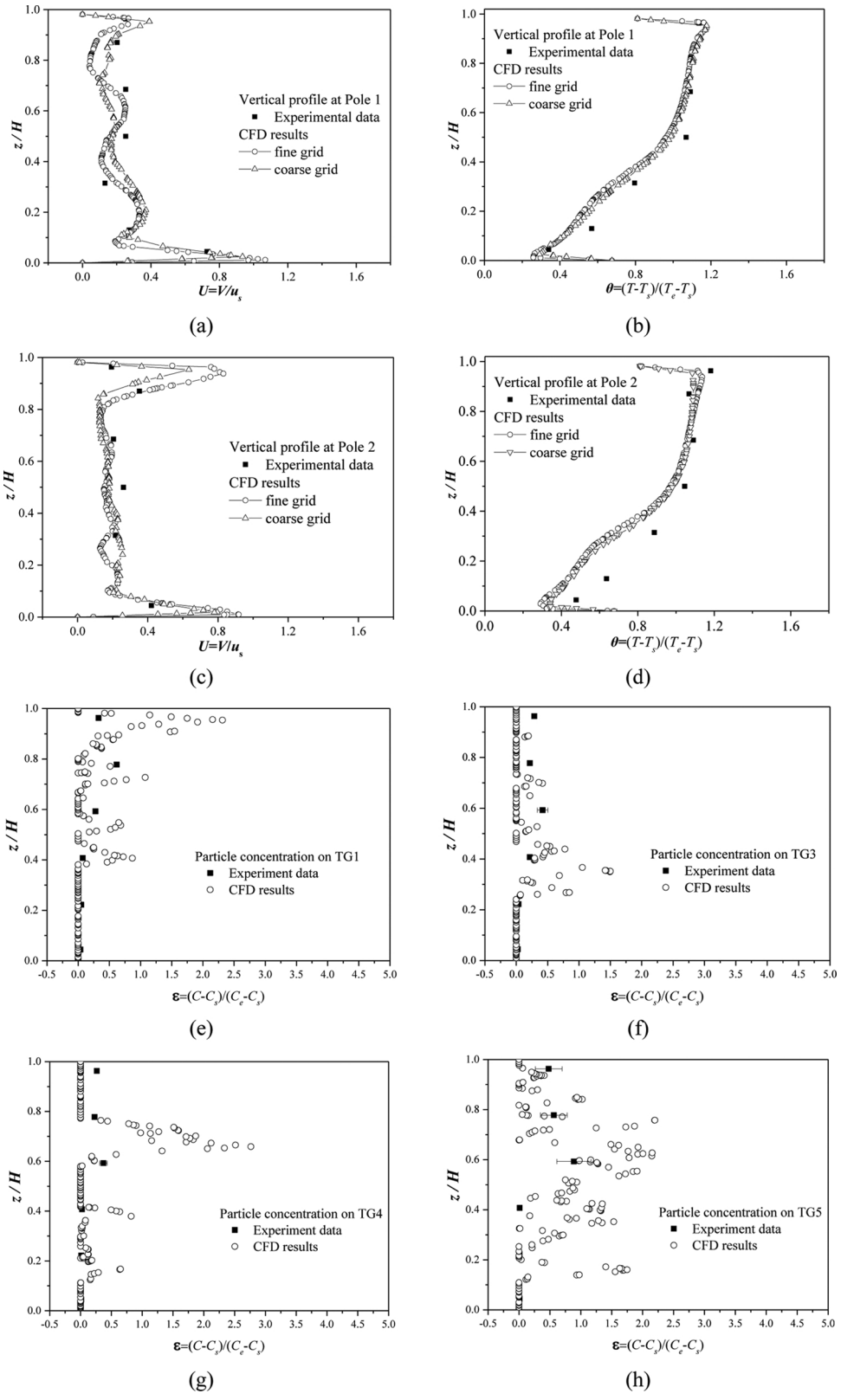

Fig. 2. Vertical profiles of normalized velocity and temperature in experiment and CFD simulation at (a-b) Pole 1, (c-d) Pole 2; Normalized particle concentration on (e) TG1, (f) TG3, (g) TG4, (h) TG5.

planes of $x = 0.315$ m and $y = 5.54$ m (Fig. 5c) where located in the air condition vents will be illustrated in the discussion section.

The fate of droplets, including suspended, deposited and escaped, as well as the number concentration of droplets around and on passengers were calculated to quantify the healthy passengers' risk of infection, which can effectively prevent and control the respiratory infectious diseases.

Table 1
Summary of CFD domain size and setup parameters of bus model.

name	number	x/m	y/m	z/m	notes
bus	1	2.6	11.63	2	\
seats	49	0.48	0.5	0.15	0.4 m from the ground, 0.83 m between the front and rear seat
seat backs	49	0.48	0.05	0.75	
luggage racks	2	0.75	9.96	0.06	1.75 m from the ground, 1.1 m between two luggage racks
exhaust	1	0.36	1.185	\	located on the top and front of the bus, above the second row seat
Air-conditioning vents	57	0.03	0.04	\	2 outlets located on the luggage racks above each seat, 9 outlets located on headstock
humans	14	\	\	\	13 passengers and 1 driver

2.3. Numerical simulation airflow model and droplet model

As is well-known, there are two main kinds of airflow patterns in nature, laminar flow and turbulent flow. Indoor airflow is usually turbulent which can be simulated by Large Eddy Simulation (LES) and Reynolds Average Navier-Stokes (RANS) turbulence models. However, the application of LES model requires longer computational time (Chen, 1995; Choi and Edwards, 2008, 2012). The Renormalization Group (RNG) k-ε turbulence model which is one of the most widely-adopted RANS models is employed in terms of accuracy, computing efficiency, and robustness for modeling indoor environments (Hang et al., 2014; Zhang and Li, 2012; Chen and Zhao, 2010; Zhang et al., 2007, 2009). Thus, we adopted the RNG k-ε model to simulate the airflow pattern in the bus. More details about the governing equations and the turbulence parameters of RNG k-ε model can be found in the literature (Hang et al., 2014; Zhang et al., 2007). The SIMPLE algorithm was adopted to decouple pressure and velocity. The second-order upwind scheme was used to discretize the convection and diffusion-convection terms in the governing equation. Besides, the Boussinesq model was employed to consider the buoyancy effect, in which the air density was regarded as a constant except in the momentum equation of vertical velocity.

Lagrangian method was used to track respiratory droplets. To simplify the calculation, the following assumptions were used:

(1) the heat and mass transfer between air and droplets were neglected;
(2) the influence of droplets on airflow was also neglected;
(3) no droplet was coagulated in its deposition process;
(4) the droplets were all in ideal sphere shape.

This approach calculates the trajectory of each droplet by solving the individual droplet movement equation whose theory is Newton's second law:

$$\frac{du_{pi}}{dt} = \sum F_i = F_{drag,i} + F_{g,i} + F_{a,i} \tag{1}$$

where u_{pi} is droplet velocity in the i direction (m/s), $\sum F_i$ is the sum of all external forces exerted on the droplet (per unit droplet mass) in i direction (m/s^2). The external forces consist of the drag force $F_{drag,i}$ (Eq. (2)), the gravity $F_{g,i}$ (Eq. (3)) and the additional forces $F_{a,i}$. According to the literature (Qian and Li, 2010; Zhang and Li, 2012; Zhao et al., 2004), the additional forces include the pressure force, virtual mass force, Basset force, Brownian force and Saffman's lift force. However, only Brownian force and Saffman's lift force were considered here since they may play an important role in sub-micron droplets' motion near walls, where the velocity gradient was large enough to make Saffman's lift force dominant, as the other forces were sufficiently small. Following the model used by the literature (Zhang and Li, 2012; Chen and Zhao, 2010), Eqs. (2) and (3) were respectively adopted to describe the drag force and gravity on the droplet in i direction:

$$F_{drag,i} = f_D/\tau_p(u_i - u_{p,i}) \tag{2}$$

$$F_{g,i} = g_i(\rho_p - \rho)/\rho_p \tag{3}$$

$$f_D(Re_p) = 1 + 0.15Re_p^{0.687} \tag{4}$$

$$\tau_p = \rho_p d_p^2 C_c/(18\mu) \tag{5}$$

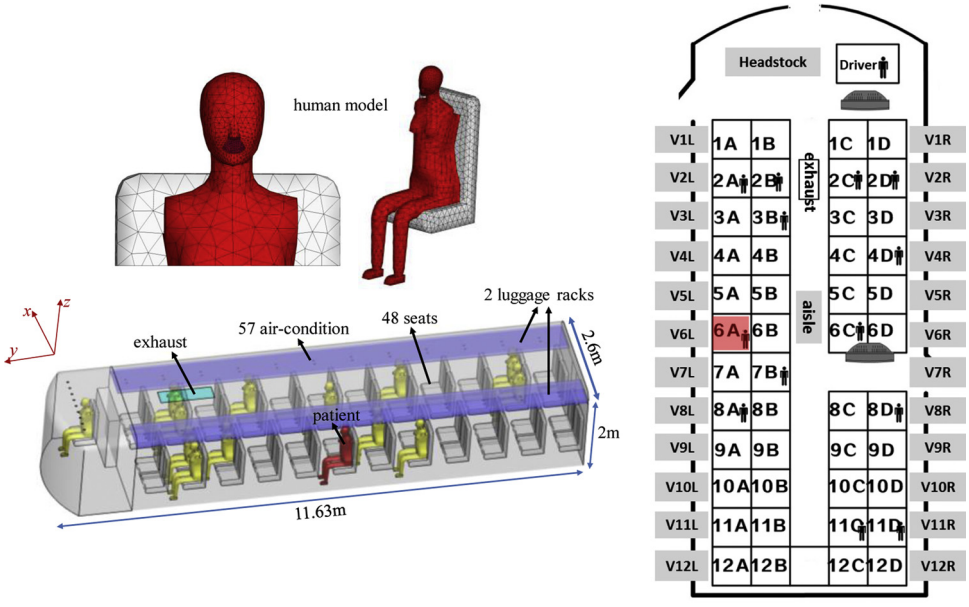

(a) (b)

Fig. 3. The computational domain, human models and the schematic structure in the coach bus.

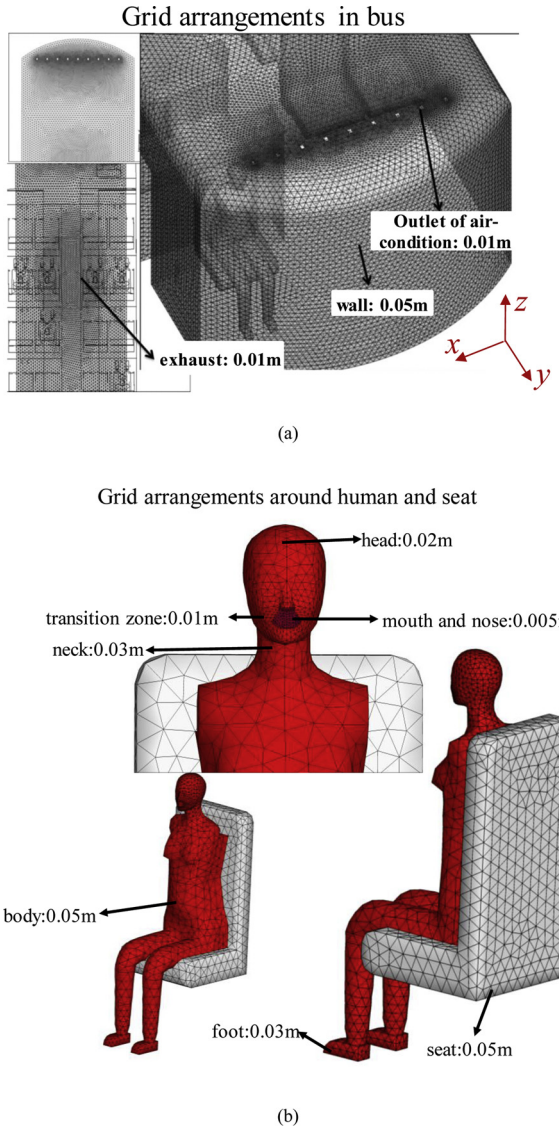

Fig. 4. The grid arrangements in the bus and around the human body and seats.

$$C_c = 1 + 2\lambda(1.257 + 0.4e^{-(1.1d_p/2\lambda)})/d_p \quad (6)$$

where f_D is the Stoke's drag modification function for large aerosol Reynolds number (Re_p) which is defined in Eq. (4); τ_p is the aerosol characteristics response time, which is defined as Eq. (5); ρ_p and ρ are respectively the density of droplet and air; d_p and μ are respectively the droplet diameter and the turbulent viscosity (kg $m^{-1}{\cdot}s^{-1}$); C_c is the Cunningham correction to Stokes drag law; λ is the molecular mean free path of air.

Respiratory droplets are composed of 90 % liquid (water) and 10 % solid elements (sodium chloride), coinciding with Potter et al. (1963). The densities of water liquid and sodium chloride are 1000 kg m^{-3} and 2170 kg m^{-3}, respectively. The density of the droplet followed the volume weighted mixing law. The specific heat followed the mass weighted mixing law. In our simulation, the default diffusion-controlled vaporization model was adopted (ANSYS Inc, 2020). The droplets evaporate till their inert content (residue) (Zhang and Li, 2012; Gupta et al., 2010). The droplet vaporization rate is defined as the following equation:

$$N_i = k_c(C_{i,s} - C_{i,sr}) \quad (7)$$

where N_i is the molar flux of vapor, kg $molm^{-2}{\cdot}s^{-1}$, and is related to the gradient of the vapor concentration between the droplet surface and the surrounding air; k_c is the mass transfer coefficient (m/s) that can be obtained using Sherwood relationship (Ranz and Marshall, 1952); $C_{i,s}$ and $C_{i,sr}$ are respectively the vapor concentration at the droplet surface and in the surrounding air (both in kg $molm^{-3}$), and can be obtained via the ideal gas relationship and molar fractions of water vapor. Droplet evaporation is influenced by RH in terms of $C_{i,sr}$ in Eq. (7).

All boundary conditions for airflow are summarized in Table 3. The influences of human breathing and heat flux at body surfaces were taken into account. Considering the total heat of 76 W (Hang et al., 2014) produced by the sleeping manikin with surface area of 1.47 m^2, the convection heat flux at body surfaces was defined as 26 W/m^2 for passengers assuming they were sedentary and 58.5 W/m^2 for the driver. For simplification, the breathing flow was assumed to be exhaled from the human mouth with the temperature of 303 K. The boundary at mouth openings (~0.0016 m^2) was set as the mean exhalation velocity of 0.12 m/s (Qian and Li, 2010; Hang et al., 2014; Liu et al., 2010) in the direction paralleling to y-axis. Our CFD simulation considered only mouth exhalation for all manikins. The air-conditioning vents were also set as velocity inlet, and the wind speed was 3.0 m/s (Air change rate per hour = 8.6 h^{-1}) with the air temperature of 290 K. Non-slip boundary conditions were applied for all walls where isothermal condition was assumed.

After the steady solutions for the airflow without droplets was obtained, the droplets were injected into the carriage through the mouth of the patient at a rate of 172 droplets per time step (for the first period, t = 0.2 s, totaling 200 iterations; for the second period, t = 1 s, totaling 560 iterations) as the airflow pattern keeps steady. After 600 s continuous releasing to get a fully-developed droplet distribution, the number of droplets exhaled from the patient was 130, 720. The Discrete Phase Boundary Conditions (DPBC) type was summarized in Table 4. For solid walls and seats, the trap condition was applied with the assumption that droplets were deposited as soon as they touch the wall surfaces and the trajectory calculation was terminated. While for the ceiling and luggage carriers, the reflect condition was set due to gravity. Escape condition was applied to the exhaust and mouths as well as air-conditioning vents.

3. Results and discussion

3.1. Droplet diffusion characteristics at different time

3.1.1. Droplet diffusion under different air-conditioning supply modes

Gravity plays a particularly important role for the movement of large droplets (50 μm) (Qian and Li, 2010; Mui et al., 2009; McGrath et al., 2019; Chao et al., 2009; Ji et al., 2018; Xie et al., 2007). Thus, to better reveal the influence of air condition supply wind, the following subsection focuses on the analysis of the 10 μm droplet diffusion in different air condition supply modes as RH = 35 %. Fig. 6 illustrates the flow field of five various air-conditioning supply modes in the surface plane of x = 0.315 m and y = 5.54 m, separately. Furthermore, Fig. 7 reveals the droplet distributions under those different indoor airflow features. As some examples, the animations of Fig. S1a-c clearly show the processes of droplet diffusion of 10 μm droplets under RH = 35 % with various supply directions (see supplementary material to this article or online at https://pan.baidu.com/s/1HVaQJzXYtSCKyUlMkk2uwg with download code 7429).

When air-conditioning supply wind blows down vertically (*Windnz*), it is obviously seen from the pictures in Fig. 6a that there are strong downward airflows from air-conditioning vents. Then a weak clockwise vortex is formed in the area between the patient and the left side wall (x = 0−0.5 m), and another weak anti-clockwise is formed in the right above the seat (x = 0.4–1.3 m). Fig. 6b reveals that, above the luggage racks, the air flows towards the headstock due to the exhausts located at the top and the front of the bus above the second-row seats. Body thermal plumes can be obviously seen around passengers. Moreover, there is a weak clockwise vortex in front of the patient. Such airflow

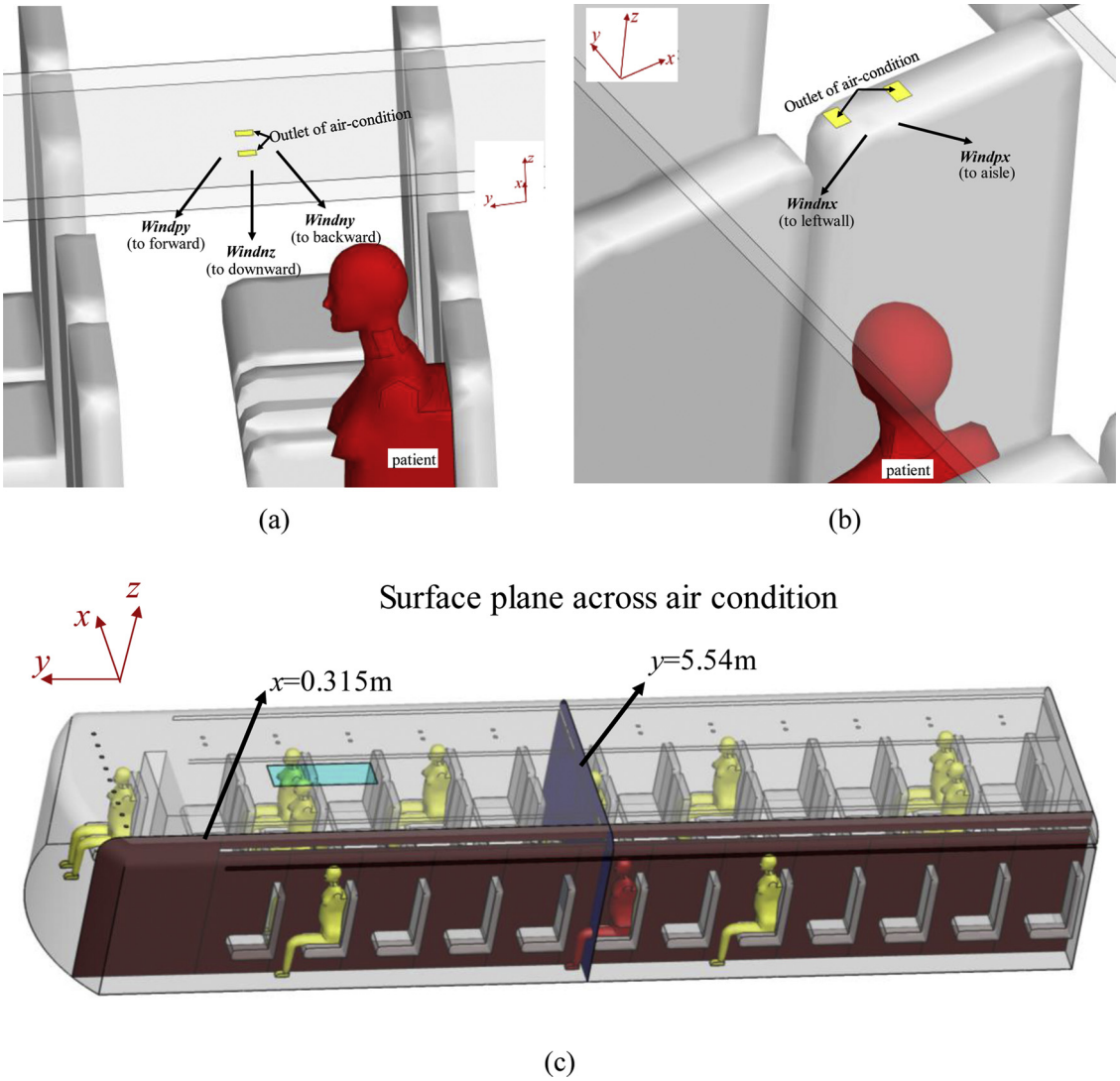

Fig. 5. The schematic of five ventilation modes (a) side view, (b) overhead view, (c) selected planes of $x = 0.315$ m and $y = 5.54$ m.

features result in the droplets diffusion in Fig. 7a1–a3 and Fig. S1a. The strong downward airflow from air-conditioning vents and gravity make droplets diffuse downwards firstly at $t = 5$ s. Droplets rise both in the left and right side of the patient through the circulation after they sink with the air-conditioning wind. Then, droplets move forwards, and diffuse more widely in the right side. Fig. 7a3 shows that there are a great number of droplets suspending in the bus. Meanwhile, many droplets are carried to the bottom of the seat, and then spread around.

There are differences between *Windnx* (Fig. 6c) and *Windpx* (Fig. 6d) supply modes as passengers will release heat and affect the flow field. Fig. 7b1–b3 and c1–c3 display the various dispersion processes. For case *Windnx* (Fig. 6c), there is a flow towards the left-side wall. Additionally, there is a flow towards the aisle under the luggage rack around the patient's head driving droplets diffuse to the center of the carriage. Therefore, droplets firstly move to the left wall with the air-conditioning supply wind (Fig. 7b1–b3), then begin to spread out to the aisle. Droplets have a time-varying tendency to diffuse to the front of the bus with the influence of exhaust fan. While for case *Windpx* (i.e. supply wind blows to the aisle, Fig. 6d), a circulation in the *xz* plane comes into being, containing an upward flow in front of the patient (*x*

Table 2
Parameters and setups in case studies.

experimental variables		variable name	Supply direction description	purpose
air condition supply modes (where p-positive, n-negative)		*Windnz*	to downward (0, 0,-1)	investigate the influence of air condition supply modes on dispersion of droplets
		Windnx	to the leftwall (-1, 0,-1)	
		Windpx	to the aisle (1, 0,-1)	
		Windny	to backward (0, -1,-1)	
		Windpy	to forward (0, 1,-1)	
liquid (water) : solid (sodium chloride) = 9:1	initial diameter of droplets	10 μm	small droplets	investigate the influence of droplets initial size on its dispersion
		50 μm	large droplets	
	environmental relative humidity (*RH*)	35 %	dry	investigate the influence of *RH* on droplets dispersion
		95 %	wet	

Table 3
Boundary conditions for airflow simulation.

boundary name	boundary conditions
air condition vents	**velocity inlet**, velocity is 3 m/s, temperature equals to 290 K, turbulent intensity is 10% various air condition supply modes in different cases
mouths and noses	**velocity inlet**, respiration rate is 0.12 m/s, temperature equals to 303 K, only consider exhale and without inhale
exhaust	**outflow**
body surface	**standard wall function, no slip wall**, heat flux is 26 W/m^2 for passengers and 58.5 W/m^2 for driver
side wall, top of bus, luggage racks	**standard wall function, no slip wall**, heat flux is 0 W/m2

= 0 − 0.5 m). As a result, after released (Fig. 7c1–c3 and Fig. S1b), droplets firstly rise up with the impact of buoyancy force and thermal plumes, and then begin to spread to the aisle and the right side of carriage due to the air-conditioning wind. During the diffusion process, there is a relatively large area with fewer obstacles. Most of the droplets spread to the right of the patient (V6R) and move forwards to V5R, and deposit on the front seat of the patient. When droplets diffuse to the right of the carriage, the circulation airflow brings droplets to aisle or the left side of the carriage under the seat, continuing to float around. In this process, a large number of droplets deposit on the surface of seats, wall and ground.

As for *Windny* (i.e. the air-conditioning wind blows to the rear of the carriage, Fig. 6e), airflow sinks when it meets seat backs, producing a vortex between the seat and the patient. There are two patterns in droplet diffusions (Fig. 7d1–d3), one is more concentrated near the left wall due to the backward moving, the other is that a small amount of droplets scatters to the aisle and fewer droplets deposit due to the small downward velocity on the right side of the patient. Over time, more and more droplets spread to the right side of bus, suspending in the air and moving towards the front of bus. Passengers 7B and 8A have a great risk of infection and passengers in the right side of the carriage are basically safe due to the small number of droplets.

The velocity is larger when air condition supply wind blows to the front of the bus (*Windpy*), which has the superposition effect with the exhaust (Fig. 6f). A vortex is formed between the patient and the front seat, where the upward flow is relatively stronger. In addition, there is also airflow across the seat backs and front. Referring to *Windpy* mode, almost half of droplets move forwards across the back of the chair, and leave several droplets sink because of small vertical downward force, and then rise up because the upward airflow continues to float to the right of the carriage (Fig. 7e1–e3 and Fig. S1c). In the process of forward diffusion, some droplets are blocked by the seat backs of V5L, and a great number of droplets move across V4L, sinking at V3L and V2L due to the obstruction of the seats subsequently. The droplet which isn't trapped in the object keeps on fluttering forwards in higher level. According to the droplet distribution at t = 40 s, there will be droplet aggregation in the front area on the left side of the bus where the patient is located.

3.1.2. Effect of the initial size of droplets on diffusion

As previously investigated (Qian and Li, 2010; Han et al., 2014; Zhang and Li, 2012; Mui et al., 2009; McGrath et al., 2019; Chao et al., 2009; Chen and Zhao, 2010; Ji et al., 2018; Xie et al., 2007), the particle/droplet dispersion process is greatly determined by the gravity force. In this study, the impacts of different initial droplet sizes and its evaporation rate are discussed. Results show that the diffusion features between 10 μm and 50 μm droplets are of great variation under the same air condition supply wind direction and *RH*. In contrast to the initial diameter of 50 μm droplets, 10 μm droplets tend to move faster, farther and wider at the same time. For example, Fig. 8 and Fig. S1c–d indicate the diffusion of droplets with different initial sizes under *RH* = 35 %, *Windpy*. As for 10 μm droplets, a great number of them move forwards across the back of the chair, and almost half of droplets and droplet nuclei diffuse in the same side of patient, affecting the passenger who is seated in the front of patient. At the meantime, the remaining half of droplets or droplet nuclei sink due to the air condition supply wind and gravity force, and subsequently float to aisle and rise up to the top of the carriage due to the airflow. The droplets diffuse in a wider range, so that they will not only gather somewhere around the sixth row. After releasing, 50 μm droplets move downwards and are mostly concentrated in the area around the patient due to the dominant role of gravity. Then, most of droplets are suspended in V6L at t = 5 s, and fewer float to V5L and aisle gradually. Particularly at t = 40 s, droplets are likely to accumulate in V5L and aisle, and diffuse to V6R. Quantities of droplets move upwards and suspend near the top of bus. In this situation, a much smaller amount of droplets diffuse to the front of the bus while passenger 6C seems in higher risk if droplets become larger.

Hence, the size of droplets determines the dominant force in the diffusion process. The larger the droplets are, the faster the deposition is, the slower the diffusion is, and the lower the risk is to the driver and passengers.

3.1.3. Effect of environment relative humidity (RH) on droplet diffusion

Relative humidity was proved to be dominant for evaporation time of droplets (Wei and Li, 2015; Liu et al., 2017). Droplets consisting of liquid (H_2O) and solid particulate matter (NaCl) was taken consideration, and the processes of evaporation and diffusion were simulated in this study. After released from patient mouth, the change of droplet size with time was counted. According to our statistics, under *RH* = 35 %, droplets with the initial diameter of 10 μm was evaporated completely within the first 0.2 s. For the condition of *RH* = 95 %, the evaporation time of 10 μm droplets hardly change, since they evaporated too fast to be seen any difference (Ji et al., 2018). As the ratio of water to sodium chloride in the droplet is set to be 9:1, the final diameter for droplets with the initial size of 10 μm and 50 μm is 3.65 μm and 18.26 μm, respectively. In another word, their volumes have been reduced to one tenth of their original size ultimately.

The change of droplet diameter under different *RH* is shown in Fig. 9. Results show that high *RH* can dramatically postpone the process of droplet evaporation, since air with higher *RH* has a lower potential in absorbing the water vapor (Ji et al., 2018). The figure reveals that the

Table 4
Boundary conditions in simulations of droplet dispersion(discrete phase).

boundary name	boundary conditions
air condition vents, exhaust, mouths and noses	**escape** (trajectory calculations are terminated here)
side wall, floor, seat surface	**trap** (trajectory calculations are terminated here)
top of bus, luggage racks	**reflect** (droplets still suspend in the air)

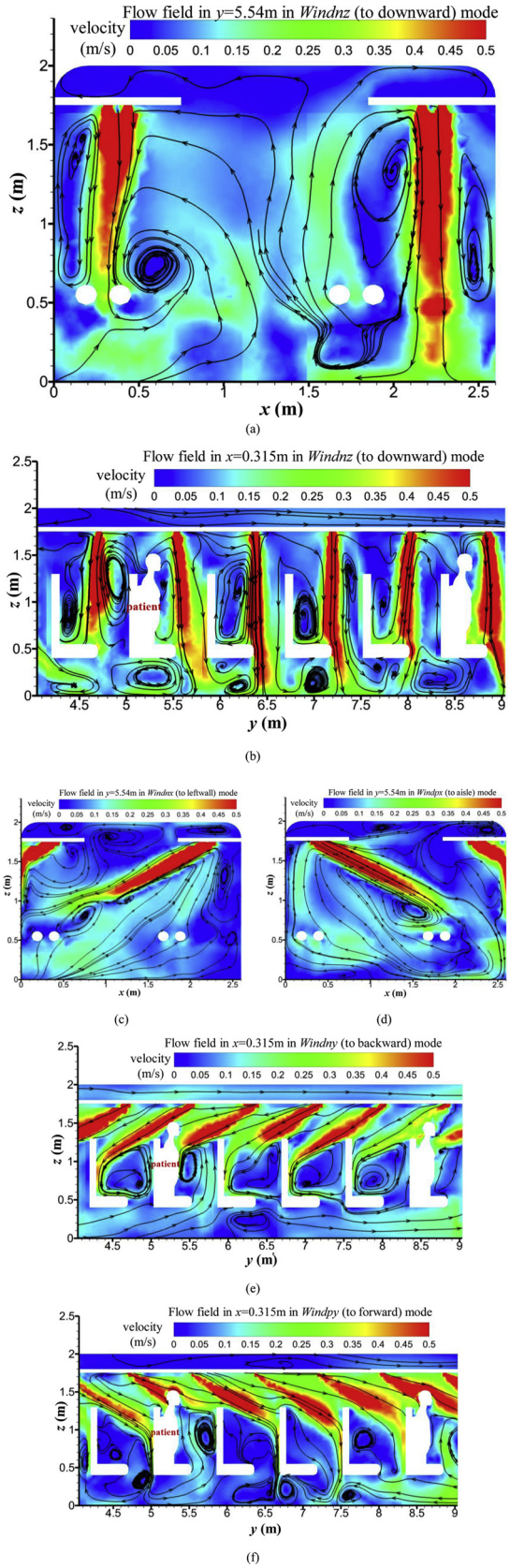

Fig. 6. Flow patterns at the selected planes: x = 0.315 m and y = 5.54 m in different modes.

droplet size decreases to stable at t = 1.8 s and 7 s respectively when RH = 35 % and 95 %. The larger the RH is, the more time it takes for droplets to evaporate. Therefore, the effect of buoyancy and gravity forces on the diffusion of droplets will be more obvious for RH = 95 %.

Nevertheless, as the short time of droplet evaporation, its influence on the diffusion of droplets is limited. Compared to 50 μm droplets, 10 μm droplets evaporate too quick to be seen any difference in the dispersion, thus 50 μm droplets are used to present to discuss as followed. Fig. 10 depicts the distribution of 50 μm droplets at different time under both dry (RH = 35 %) and wet (RH = 95 %) environment in the *Windny* mode. In general, droplets seem to move towards the same direction, and the dispersion range has no significant variation between them. Actually, as a result of the short evaporation time (1.8 s) in RH = 35 %, droplets shrink quickly to droplet core whose diameter is 18.26 μm, and subsequently diffuse fast. It is observed in Fig. 10a2, a3 and b2, b3 that droplets arrive the farther place compared to RH = 95 %. Besides, it should be mentioned that the number of droplets in RH = 95 % is fewer than that in RH = 35 %, because more droplets will deposit in the object surface in the diffusion process, leading to less suspension droplets (e.g. *Windpy*, Fig. S1d–e), which will be discussed in Section 3.2.

3.2. Ultimate fate of droplets with various initial diameters, ventilation and RH

3.2.1. Ratio of droplets eventually trapped, suspended and escaped

After released from the patient' mouth, droplets begin to evaporate and spread to every corner of the carriage because of the gravity, buoyancy force and airflow of the air-conditioning. In this paper, droplets composed of liquid and solid elements are employed. The solid elements still travel around in the carriage after the liquid is evaporated. During the diffusion process, some droplets' journey will end up when they deposit on the surface of the seats, human bodies or walls, while the others still suspend till they deposit or escape from the exhaust fan which is set on the front of the roof. In general, there are three final statuses of droplets when the calculation stops, named trapped, suspended and escaped, and the total number of them is 130,720.

Fig. 11 depicts the proportion of droplets which are eventually trapped, suspended and escaped from the carriage in five different air-conditioning supply directions and two RH environments with initial droplet size of 10 μm and 50 μm. All cases have the same total amount of droplets, and the sum of the proportion of droplets in the aforementioned three states is 100 %. Note that all the ordinates start at 80 %.

Most of droplets (more than 84 %) are trapped on the surface of seats, passengers and walls. Moreover, the amount of trapped, suspended and escaped droplets varies significantly under different wind directions. For 10 μm droplets (blue bars), number of droplets depositing on objects is the largest when air condition supply wind blows towards the rear of the bus (*Windny*, ~95.2 %), followed by toward headstock (*Windpy*, ~92.5 %), and smallest while that supply wind blows downwards (*Windnz*, ~85.1 %) and towards the left wall (*Windnx*, ~85.0 %). The proportion of droplets suspending in the air under the circumstance of *Windpx* and *Windnx* is up to 5.6–6.0 %, which is about two times more than that under the *Windpy* mode. The proportion of droplets escaped from the carriage in the *Windnz* mode is largest (10.4 %), and followed by in the mode of *Windnx* (9.4 %), *Windpx* (7.3 %), and *Windpy* (4.1 %). Even less droplets are escaped (1.3 %) in the mode of *Windny*, because the supply wind blows to the rear of the bus, which is the opposite direction of the exhaust fan.

In addition, when the droplet size increases to 50 μm (orange bars), the effect of wind direction becomes smaller than that for 10 μm droplets. As a result, more than 91.0 % of 50 μm droplets will deposit. The proportion of suspended droplets decreases slightly from 3.5 to 6.0% (10 μm) to 1.3–4.5 % (50 μm) due to the greater gravity force on larger droplets. There is an exception that the proportion of suspended

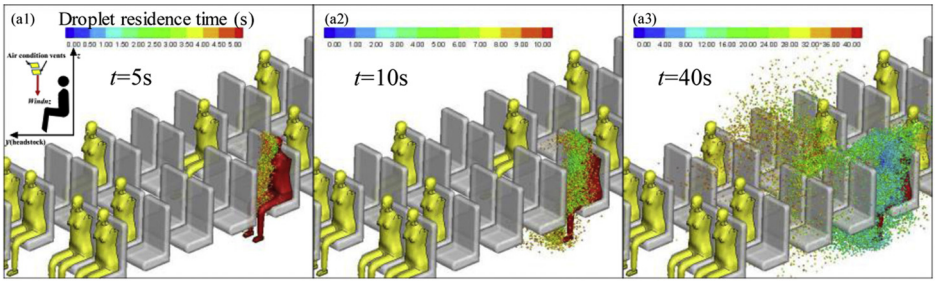

10μm droplets under *RH*=35% and ***Windnz*** (to downward)

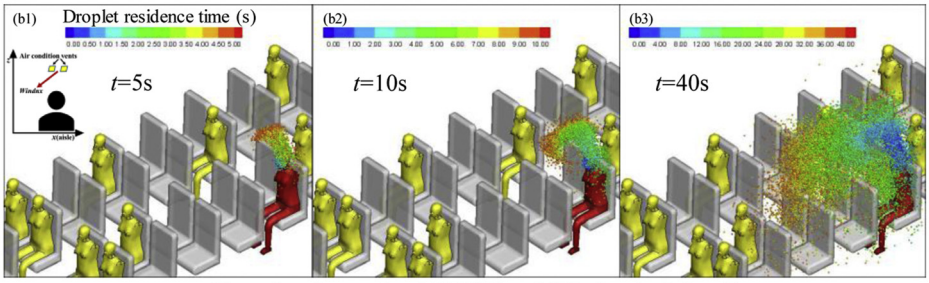

10μm droplets under *RH*=35% and ***Windnx*** (to leftwall)

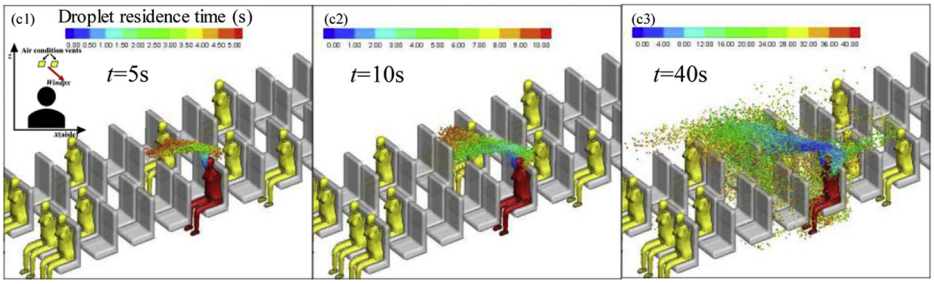

10μm droplets under *RH*=35% and ***Windpx*** (to aisle)

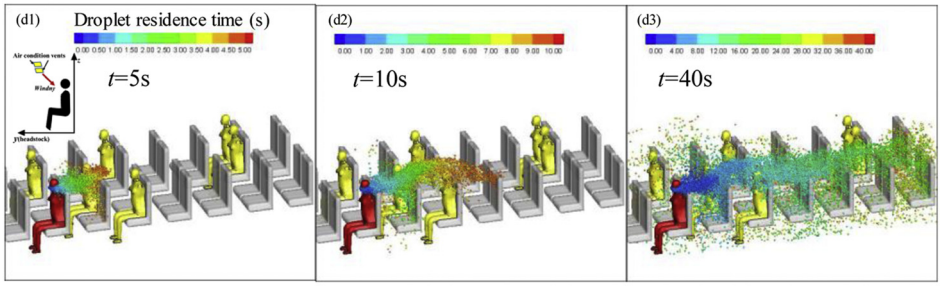

10μm droplets under *RH*=35% and ***Windny*** (to backward)

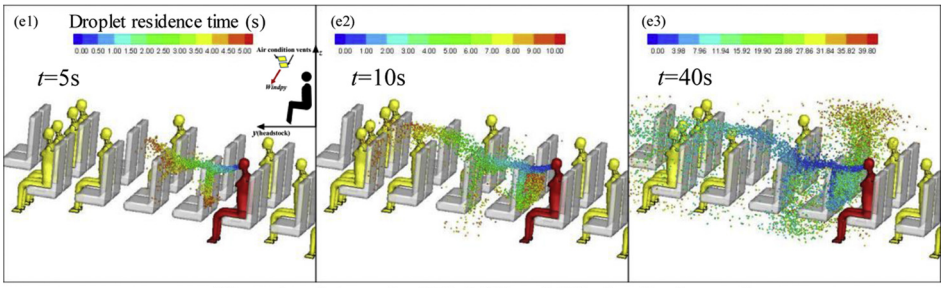

10μm droplets under *RH*=35% and ***Windpy*** (to forward)

Fig. 7. Distribution of 10 μm droplets at different time with *RH* = 35 % and five air-conditioning supply modes(droplet color indicates its existence time): (a1-3) *Windnz*(to downward), (b1-3) *Windnx*(to leftwall), (c1-3) *Windpx*(to aisle), (d1-3) *Windny*(to backward), (e1-3) *Windpy*(to forward).

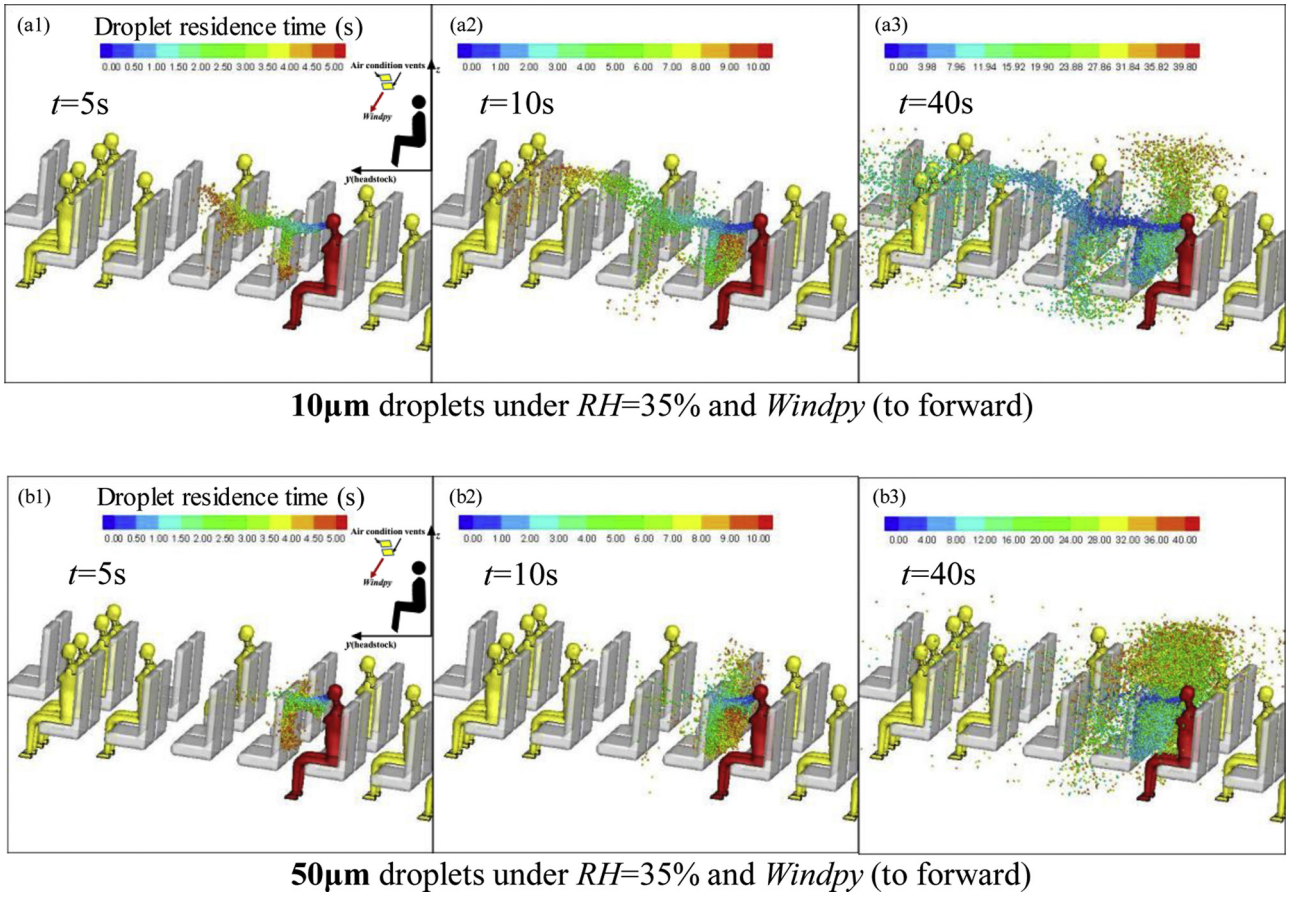

Fig. 8. Droplets distribution at different time under *RH* = 35 % and *Windpy* (to forward) supply mode (droplet color indicates the existence time of droplets.) (a1-3) 10 μm, (b1-3) 50 μm.

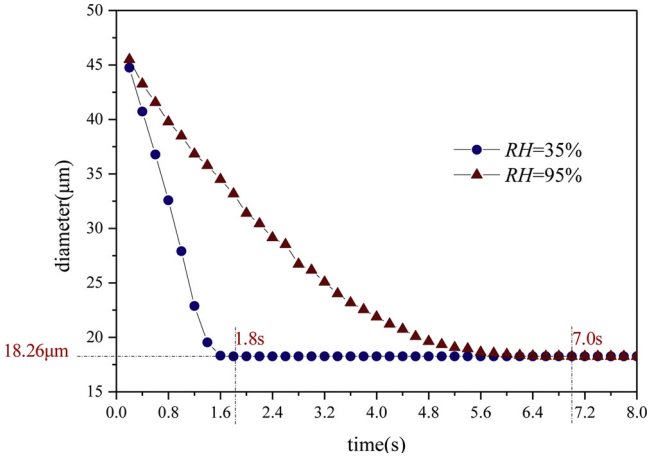

Fig. 9. The variation of diameter for droplets with initial size of 50 μm due to evaporation.

droplets increases from 3.2 to 3.4% (10 μm) to 6.9–8.5 % (50 μm) in the mode of *Windpy* where droplets are stopped by the V5L seat backs and move towards the aisle with little obstruction. However, the number of escaped droplets is of dramatically reduction, especially in the *Windny* mode, which decreases to 0.04 %. As the initial diameter increased, droplets are less removed from the carriage, and most of them still stay in the bus, which is a risk to passengers.

When the relative humidity is between 35 % and 95 %, droplets express similarity in their ultimate fate. There is slight distinction of fate for 50 μm droplets in different conditions of supply wind, which is related to the short evaporation time of 10 μm. Taking 50 μm droplet as an example, in the mode of *Windpy*, 6.9 % and 8.5 % of droplets are suspended when *RH* = 35 % and 95 %, respectively. The relative humidity brings the same function to droplets size. Therefore, the influence of *RH* on dispersion of droplets depends on the initial size of droplets and the supply wind direction.

3.2.2. Droplet distribution characteristics in different volumes

The possibility of passenger infection depends largely on the temporal distribution characteristics of droplets exhaled from the infected source patient. The modeled bus is divided into 27 zones as shown in Fig. 3b, including headstock, aisle, roof and the other 24 zones separated by the seats. The volumes on the left side of the infected individual are numbered as V1L to V12 L, and the others are numbered as V1R to V12R. The number of suspended droplets located in the 27 zones is counted to present the droplet temporal distribution features. Figures show the temporal distribution of droplets with diameters of 10 μm (Fig. 12a) and 50 μm (Fig. 12b) under different environment. The *x* axes represent the Volume No. defined above. The *y* axes represent the $\varepsilon_{suspend}=N_{s,i}/N_t$, where $N_{s,i}$ and N_t are the suspended droplet number in Volume No. *i* and total number released by patient respectively.

Fig. 12a summarizes suspended droplets in the carriage under *RH* = 35 % due to the similar distribution between different relative humidity. The overall temporal distribution characteristics of 10 μm droplets are summarized as follows. The change of *RH* seems to be little impact on droplet dispersion, such influence is embodied that $\varepsilon_{suspend}$ discrepancy varies from -0.37‰ to 0.54‰ between *RH* = 35 % and 95 %. There is a similar droplet distribution of left side volumes in the modes of *Windnz* (to downward), *Windnx* (to the left wall), *Windpx* (to the aisle) and *Windpy* (to forward). V6L, where the patient is located in,

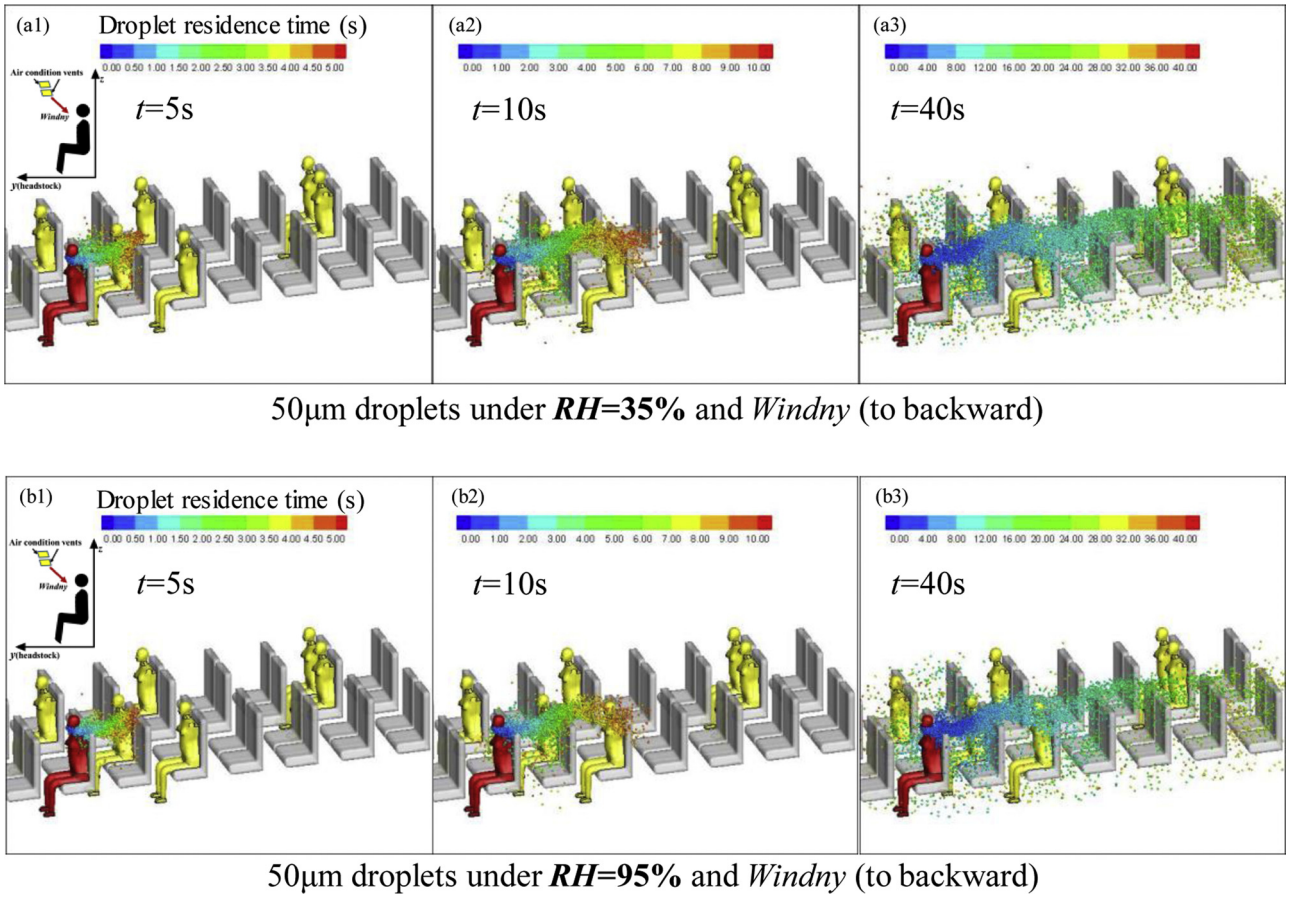

Fig. 10. Initial size of 50 μm droplets distribution at different times under *Windny* (to backward) air-conditioning supply mode (droplet color indicates the existence time of droplets.) (a1-3) *RH* = 35 %, (b1-3) *RH* = 95 %.

appears the maximum quantity (6.36‰-16.82‰). Some droplets disperse to the other side because of the circulation airflow pattern as the exhaust is located on the ceiling near the headstock in the coach bus. Some droplets are transmitted by the forward airflow to the front of the coach bus. Besides, there are some apparent differences for the case of *Windny* (to backward), substantial droplets will suspend in zones behind patient (V7L-V12 L). Droplets tend to diffuse to the aisle and the right-side areas in the mode of *Windpx*, thus their distribution is

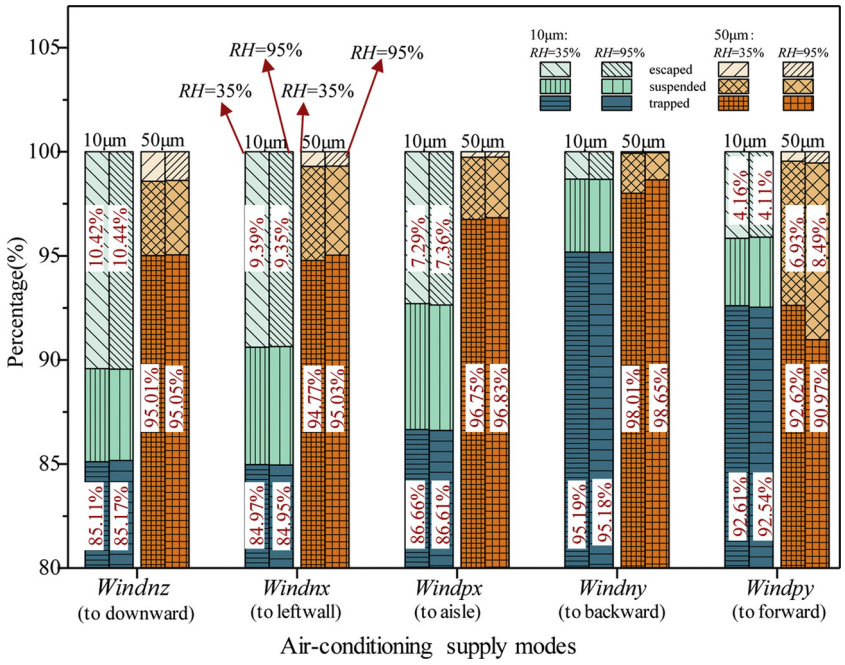

Fig. 11. The ultimate fate of droplets with different initial size under various air supply directions and *RH*.

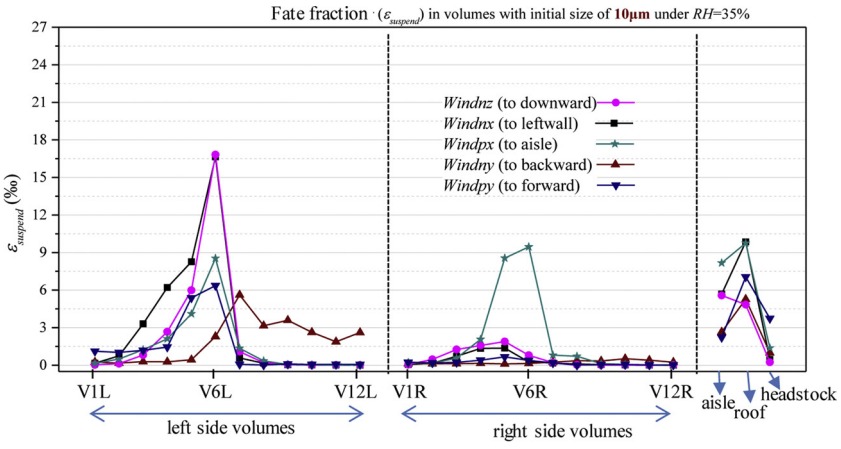

(a)

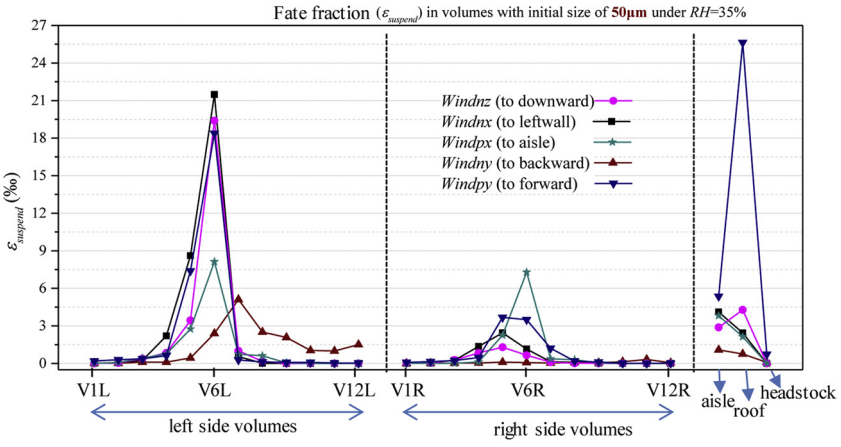

(b)

Fig. 12. Temporal distribution of droplets with different sizes: (a) 10 μm, (b) 50 μm under RH = 35 % in the 27 zones.

relatively even on both sides. Such characteristics lead to higher risk in the front zones at the same side of patient comparing to other zones except for the *Windny* mode.

In contrast to 10 μm droplets, 50 μm droplets are limited to spread around the patient and accumulate in the regions including V5L-V6L and V5R-V6R. Especially for *Windnz*, *Windnx*, *Windpy*, there are over 18.38‰ of droplets and droplet nuclei gathering in V6L, subsequently decrease in the front and back of patient. In particular, 50 μm droplets are hardly diffuse to V1L-V3L where several 10 μm droplets can arrive, because the former deposit first when meet the obstructions. More 50 μm droplets can float to aisle and further to V4R-V7R. When the air-conditioning wind blows to the front of the bus (*Windpy*), there are 25.63‰ of 50 μm droplets suspended in the "roof" zone, which is more than 10 μm droplets (7.06‰). Droplets mostly suspend above the fifth and sixth row. This result is consistent with the previous droplet diffusion characteristics in subsection 3.1.1.

3.2.3. Droplets trap on each passenger

Passengers whose body surfaces are deposited by droplets exhaled from the source patient are at higher risk to get infected than those whose body surfaces are not deposited. Thus, fate fraction $\varepsilon_{trap}=N_{t,i}/N_t$ is defined, where $N_{t,i}$ and N_t are the number deposit in passenger i and the total number released by the index patient, was calculated to quantified the droplet deposited on subject surface, and try to correlate the infection risk of passengers. Table 5 shows the ε_{trap} on each passenger.

Passengers who are in front of or on the same row with the source patient tend to get infected if the droplets size is small (10 μm), e.g. 6C who seat in the right side of patient of the sixth row, ε_{trap} ~ 0.5–22.4, has a higher risk under different air-conditioning supply direction. Passenger 7B and 8A who are seated behind the source patient, experience 13.4 and 21.2 of ε_{trap} respectively, are easier to get infected if the air-conditioning wind blow to the rear of bus (*Windny*). The infection potential for passengers 2A ~ 2D, 3B who seat in front of the patient has a lower risk when the droplet diameter is 50 μm compared to 10 μm. More droplets will deposit on the passengers around the patient such as 6C, 7B. In terms of driver and passenger 11C and 11D, the distance between them and patient is more than 4.5 m, which significantly reduce the probability of airborne transmission.

Finally, we recall the facts that no passengers were infected by the source patient with MERS from South Korea. Several reasons can be the most significant. First, although the source patient did not wear any mask, fortunately he did not cough/sneeze or talk with other people. There were only droplets exhaled by breathing activities. Second, it was lucky that there were no passengers in the adjacent seats in front of or behind this source patient as well as beside his seat which were revealed of the highest risk for droplet transmission. For the other seats, the risk of droplet transmission decreased sharply.

4. Limitations and future research

Our study can be further improved in which more processes/

Table 5
Fate fraction ε_{trap} (‰) of 10 μm and 50 μm droplets on each passenger under RH = 35 %.

	Windnz		*Windnx*		*Windpx*		*Windny*		*Windpy*	
	10 μm	50 μm	10 μm	50 μm	10 μm	50 μm	10 μm	50 μm	10 μm	50 μm
6A,patient	151.9	201	210.5	216.1	122.4	136.8	202.6	136.6	6.1	12.3
driver	0.1	0	0.1	0	0.4	0	1.4	0	0.8	0.2
2A	0.7	0.2	2.9	0.2	0.7	0.2	0.5	0	7.6	1.1
2B	0.3	0.2	2	0.2	1.4	0.3	0.5	0.1	2.5	0.4
2C	1.2	0.4	0.9	0	0.9	0.1	0.3	0	0.3	0.1
2D	2	0.7	0.2	0	0.3	0	0.2	0	0.4	0.3
3B	3	2.1	4.4	0.7	3	0.9	0.9	0.4	1.9	0.8
4D	4.5	3.5	2	4.1	5.8	0.2	0.3	0	2.3	2.8
6C	5.7	6.8	0.9	4.6	22.4	21.5	0.5	0.3	0.5	6.5
7B	1.1	1.5	1	2.2	4.4	2.1	13.4	11.6	0.3	1.8
8A	1.6	1.1	0.4	0.1	0	0.4	21.2	25	0.1	0.3
8D	0.3	0	0	0.1	4.6	2.7	1.1	0.2	0	0.4
11C	0	0	0	0	0	0	1.7	2.3	0	0
11D	0	0	0	0	0	0	0.4	0.1	0	0

parameters are considered. Firstly, we only studied the influence of air-conditioning wind direction and relative humidity on the droplet dispersion. However, in real cases, the location of the infection source relative to the exhaust fan is also an important factor on the droplet diffusion, transmission, and elimination, because the only exhaust fan is of great significance on flow pattern in the enclosed bus. Secondly, as a start, this study only considered exhaled droplet by breathing. Future investigations will consider different respiratory activities (e.g. speaking, coughing, sneezing), which may lead to complex jet speed and different initial characteristics of droplets (sizes, velocities etc.). Thirdly, the final fate and composition of the droplets are of great significance for the evaluation of the infection risk, and the relationship between them deserves further study.

5. Conclusion

The enclosed and crowded indoor environments in long-route coach buses usually experience high infection risk of respiratory diseases due to droplet transmissions. In this study, as a novelty, we built a numerical model according to a real case to investigate the influence of ventilation and evaporation of exhaled droplets on their transport. We employed five air supply directions, two kinds of relative humidities (RH = 35 % and 95 %) and initial droplet sizes (10 μm and 50 μm). We summarized the number of droplets/droplet nuclei suspending in different zones and depositing on the body surface of each passenger to show the temporal and spatial characteristics of droplet distributions.

Some meaningful findings are addressed:

(1) Droplets with the initial diameter of 10 μm finish evaporation within the first 0.2 s as RH = 35 % and 95 %, while 50 μm droplets evaporate to pure solid droplet nuclei within 1.8 s and 7.0 s respectively under dry and wet conditions.
(2) Followed by the air supply mode and droplet initial size, droplet evaporation related to relative humidity is the third key factor influencing the droplet diffusion and its final state. RH of 95 % tends to attain less risk of droplet transmission than RH of 35 % because droplets evaporate slower in wetter air and deposit more quickly onto wall surfaces.
(3) In general, small droplets (10 μm) diffuse faster, farther and wider compared with large droplets (50 μm). 91 %–100 % of 50 μm droplets are trapped on the surfaces, which is higher than that of 10 μm (85 %–95 %) because of the gravity-force effects.
(4) Most of droplets distributed on one side of the infected individual than on the other side (more than about 0.07‰-7.65‰) except for the case of *Windpx* (to the aisle). The arrangement of exhaust fan results in the higher risk for passengers in front rows of the patient (i.e. regions near the exhaust fan).
(5) The region behind the patient is of higher infection risk only in the mode of *Windny* (to backward), meanwhile droplets would like to suspend in the air in the mode of *Windpx* (to the aisle) when droplets spread to the widest region.

Therefore, we conclude that it is necessary to clean the car regularly and keep the bus tidy since there are more droplets deposited on the surface of the object. Moreover, relatively wet environment is conducive to control the diffusion and propagation of droplets and droplet nuclei. In addition, in order to reduce the transmission of infectious disease virus in the period of respiratory infectious diseases, besides wearing masks, risk of droplet transmission may decrease sharply if passengers sit at nonadjacent seats because most droplets can only travel a limited distance from the source patient. It is also necessary to effectively use the better ventilation mode in the public transport, i.e. the *Windny* mode (supply to bus backward) for which most droplets deposit onto surfaces is recommended in the long-route coach bus in this study. Although further investigations are still required before providing practical guidelines, this paper is one of the first attempts to assess the impacts of ventilation modes and relative humidity on droplet transmissions in the enclosed coach bus environment which can provide a physical basis for further prediction of passenger infection rate.

Credit author statement

Miss Xia Yang performed numerical simulation and data analysis. Miss Hongyu yang helped Miss Xiayang in making models. Dr Cuiyun Ou contributed to paper writing and Prof Jian Hang lead this research with paper submission. Dr Li Liu helped in the model of droplet evaporation. Mr Tie Song, Min Kang and Dr Hualiang Lin provided the measured data of ventilation rates and passenger arrangements etc in the real bus coach in MERS period of 2015.

Declaration of Competing Interest

The authors declare that they have no known competing financial interests or personal relationships that could have appeared to influence the work reported in this paper.

Acknowledgements

This study was financially supported by National Key Research and Development Program of China [grant numbers 2016YFC0202206, 2016YFC0202205 and 2016YFC0202204], the National Natural Science Foundation of China (grant number. 51811530017 and

41875015) and STINT, Sweden (grant number dnr CH2017-7271) as well as the Key projects of Guangdong Natural Science Foundation, China (grant number 2018B030311068) and Special Fund (International Cooperation) Project for Science and Technology Innovation Strategy of Guangdong Province, China (grant number 2019A050510021), China Postdoctoral Science Foundation (No. 2019M653147). The supports by National Supercomputer Center in Guangzhou, P.R. China and the help from Miss Qiaoling Ren, Miss Tianying Liu are also gratefully acknowledged.

Appendix A. Supplementary data

Supplementary material related to this article can be found, in the online version, at doi:https://doi.org/10.1016/j.jhazmat.2020.122609.

References

ANSYS Inc, 2020. ANSYS FLUENT User's Guide, (version 15.0).
Bartzis, J.G., Efthimiou, G.C., Andronopoulos, S., 2015. Modelling short term individual exposure from airborne hazardous releases in urban environments. J. Hazard. Mater. 300, 182–188.
Cao, G., Nielsen, P.V., Jensen, R.L., Heiselberg, P., Liu, L., Heikkinen, J., 2015. Protected zone ventilation and reduced personal exposure to airborne cross-infection. Indoor Air 25, 307–319.
Castle, M., Wiley, A., 1987. Hospital infection control: principles and practice. J. Hosp. Infect. 13 (1), 104.
Chao, C.Y.H., Wan, M.P., Morawska, L., Johnson, G.R., Ristovski, Z.D., Hargreaves, M., Corbett, S., Li, Y.G., Xie, X.J., Katoshevski, D., 2009. Characterization of expiration air jets and droplet size distributions immediately at the mouth opening. J. Aerosol Sci. 40 (2), 122–133.
Chen, Q.Y., 1995. Comparison of different models for indoor airflow computation. Numer. Heat Transf. Part B Fundam. 28, 353–369.
Chen, C., Zhao, B., 2010. Some questions on dispersion of human exhaled droplets in ventilation room: answers from numerical investigation. Indoor Air 20 (2), 95–111.
Choi, J.I., Edwards, J.R., 2008. Large eddy simulation and zonal modeling of human-induced contaminant transport. Indoor Air 18, 233–249.
Choi, J.I., Edwards, J.R., 2012. Large-eddy simulation of human-induced contaminant transport in room compartments. Indoor Air 22 (1), 77–87.
Gupta, J.K., Lin, C.H., Chen, Q.Y., 2010. Characterizing exhaled airflow from breathing and talking. Indoor Air 20 (1), 31–39.
Gupta, J.K., Lin, C.H., Chen, Q.Y., 2012. Risk assessment of airborne infectious diseases in aircraft cabins. Indoor Air 22 (5), 388–395.
Han, Z.Y., Sze To, G.N., Fu, S.C., Chao, C.Y.H., Weng, W.G., Huang, Q.Y., 2014. Effect of human movement on airborne disease transmission in an airplane cabin: study using numerical modeling and quantitative risk analysis. BMC Infect. Dis. 14 (1), 1–19.
Hang, J., Li, Y.G., Jin, R.Q., 2014. The influence of human walking on the flow and airborne transmission in a six-bed isolation room: tracer gas simulation. Build. Environ. 77, 119–134.
Hang, J., Li, Y.G., Ching, W.H., Wei, J.J., Jin, R.Q., Liu, L., Xie, X.J., 2015. Potential airborne transmission between two isolation cubicles through a shared anteroom. Build. Environ. 89, 264–278.
Ji, Y.C., Qian, H., Ye, J., Zheng, X.H., 2018. The impact of ambient humidity on the evaporation and dispersion of exhaled breathing droplets: a numerical investigation. J. Aerosol Sci. 115, 164–172.
Kao, P.H., Yang, R.J., 2006. Virus diffusion in isolation rooms. J. Hosp. Infect. 62 (3), 0–345.
Kowalski, W., Bahnfleth, W., 1998. Airborne respiratory diseases and mechanical systems for control of microbes. Heat. Piping Air Cond. 70 (7), 34–48.
Lai, A.C.K., Cheng, Y.C., 2007. Study of expiratory droplet dispersion and transport using a new Eulerian modeling approach. Atmos. Environ. 41 (35), 7473–7484.
Lai, A.C.K., Poon, C.K.M., Cheung, A.C.T., 2012. Effectiveness of facemasks to reduce exposure hazards for airborne infections among general populations. J. R. Soc. Interface 9 (70), 938–948.
Li, Y.G., Ching, W.H., Qian, H., Yuen, P.L., Seto, W.H., Kwan, J.K.C., Leung, M., Yu, S.C.T., 2007. An evaluation of the ventilation performance of new SARS isolation wards in nine hospitals in Hong Kong. Indoor Built Environ. 16 (5), 400–410.
Lidwell, O.M., Williams, R.E.O., 1961. The epidemiology of the common cold. Epidemiol. Infect. 59 (3), 309–319.
Liu, P., Wang, B.B., Zhao, X.G., Duan, X.L., Huang, N., Chen, Y.T., Wang, L.M., 2010. Research on inhalation rate of Chinese adults. J. Environ. Health 31 (11), 953–956 (in Chinese).
Liu, X.P., Niu, J.L., Kwok, K.C.S., 2011a. Analysis of concentration fluctuations in gas dispersion around high-rise building for different incident wind directions. J. Hazard. Mater. 192, 1623–1632.
Liu, X.P., Niu, J.L., Kwok, K.C.S., Wang, J.H., Li, B.Z., 2011b. Local characteristics of cross-unit contamination around high-rise building due to wind effect: mean concentration and infection risk assessment. J. Hazard. Mater. 192, 160–167.
Liu, L., Wei, J.J., Li, Y.G., Ooi, A., 2017. Evaporation and dispersion of respiratory droplets from coughing. Indoor Air 27 (1), 179–190.
Mazumdar, S., Poussou, S.B., Lin, C.H., Isukapalli, S.S., Plesniak, M.W., Chen, Q.Y., 2011. Impact of scaling and body movement on contaminant transport in airliner cabins. Atmos. Environ. 45, 6019–6028.
McGrath, J.A., O'Sullivan, A., Bennett, G., O'Toole, C., Joyce, M., Byrne, M.A., MacLoughlin, R., 2019. Investigation of the quantity of exhaled aerosols released into the environment during Nebulisation. Pharmaceutics 11 (2), 1–9.
Mui, K.W., Wong, L.T., Wu, C.L., Lai, A.C.K., 2009. Numerical modeling of exhaled droplet nuclei dispersion and mixing in indoor environments. J. Hazard. Mater. 167 (1–3), 736–744.
Pereira, J.C.F., Chen, X.Q., 1996. Numerical calculations of unsteady heavy gas dispersion. J. Hazard. Mater. 46 (2-3), 253–272.
Potter, J.L., Matthews, L.W., Lemm, J., Spector, S., 1963. Human pulmonary secretions in health and disease. Ann. N. Y. Acad. Sci. 106, 692–697.
Qian, H., Li, Y.G., 2010. Removal of exhaled particles by ventilation and deposition in a multibed airborne infection isolation room. Indoor Air 20 (4), 284–297.
Qian, H., Li, Y.G., Nielsen, P.V., Hyldgaard, C.E., Wong, T.W., Chwang, A.T.Y., 2006. Dispersion of exhaled droplet nuclei in a two-bed hospital ward with three different ventilation systems. Indoor Air 16 (2), 111–128.
Ranz, W.E., Marshall, W., 1952. Evaporation from drops, Part II. Chem. Eng. Progress 48 (3), 173–180.
Saravia, S.A., Raynor, P.C., Streifel, A.J., 2007. A performance assessment of airborne infection isolation rooms. Am. J. Infect. Control 35 (5), 0–331.
Scargiali, F., Grisafi, F., Busciglio, A., Brucato, A., 2011. Modeling and simulation of dense cloud dispersion in urban areas by means of computational fluid dynamics. J. Hazard. Mater. 197, 285–293.
Shih, Y.C., Chiu, C.C., Wang, O., 2007. Dynamic airflow simulation within an isolation room. Build. Environ. 42 (9), 3194–3209.
Sung, M., Jo, S., Lee, S.E., Ki, M., Choi, B.Y., Hong, J., 2018. Airflow as a possible transmission route of middle east respiratory syndrome at an initial outbreak hospital in Korea. Int. J. Environ. Res. Public Health 15 (12), 1–11.
Tung, Y.C., Hu, S.C., Tsai, T.I., Chang, I.L., 2009. An experimental study on ventilation efficiency of isolation room. Build. Environ. 44 (2), 271–279.
Wang, C., Holmberg, S., Sadrizadeh, S., 2018. Numerical study of temperature-controlled airflow in comparison with turbulent mixing and laminar airflow for operating room ventilation. Build. Environ. 144, 45–56.
Wei, J.J., Li, Y.G., 2015. Enhanced spread of expiratory droplets by turbulence in a cough jet. Build. Environ. 93, 86–96.
Wei, J.J., Zhou, J., Cheng, K., Wu, J., Zhong, Z.F., Song, Y.C., Ke, C.W., Yen, H.L., Li, Y.G., 2018. Assessing the risk of downwind spread of avian influenza virus via airborne particles from an urban wholesale poultry market. Build. Environ. 127, 120–126.
Wong, T.W., Lee, C.K., Tam, W., Lau, T.F., Yu, T.S., Lui, S.F., Chan, K.S., Li, Y.G., Bresee, S., Sung, J.Y., Parashar, D., 2004. Cluster of SARS among medical students exposed to single patient, Hong Kong. Emerging Infect. Dis. 10 (2), 269–276.
World Health Organization, 2020a. Disease Outbreaks. (Accessed 5 February 2020). https://www.who.int/emergencies/diseases/en/.
World Health Organization, 2020b. Novel Coronavirus (2019-nCoV) Situation Reports. (Accessed 5 February 2020). https://www.who.int/emergencies/diseases/novel-coronavirus-2019/situation-report/.
Xie, X.J., Li, Y.G., Chwang, A.T.Y., Ho, P.L., Seto, W.H., 2007. How far droplets can move in indoor environments-revisiting the Wells evaporation-falling curve. Indoor Air 17 (3), 211–225.
Xie, X.J., Li, Y.G., Sun, H.Q., Liu, L., 2009. Exhaled droplets due to talking and coughing. J. R. Soc. Interface 6, 703–714.
Xu, C., Nielsen, P.V., Gong, G., Liu, L., Jensen, R.L., 2015. Measuring the exhaled breath of a manikin and human subjects. Indoor Air 25, 188–197.
Yan, W., Zhang, Y., Sun, Y., Li, D., 2009. Experimental and CFD study of unsteady airborne pollutant transport within an aircraft cabin mock-up. Build. Environ. 44 (1), 34–43.
Yang, S., Lee, G.W.M., Chen, C.M., Wu, C.C., Yu, K.P., 2007. The size and concentration of droplets generated by coughing in human subjects. J. Aerosol Med. 20 (4), 484–494.
Yin, Y., Xu, W., Gupta, J.K., Guity, A., Marmion, P., Manning, A., Gulick, R.W., Zhang, X., Chen, Q., 2009. Experimental study on displacement and mixing ventilation systems for a patient ward. HVACR Res. 15, 1175–1191.
Yu, I.T.S., Li, Y.G., Wong, T.W., Tam, W., Chan, A.T., Lee, J.H.W., Leung, D.Y.C., Ho, T., 2004. Evidence of airborne transmission of the severe acute respiratory syndrome virus. N. Engl. J. Med. 350 (17), 1731–1739.
Zhang, L., Li, Y.G., 2012. Dispersion of coughed droplets in a fully-occupied high-speed rail cabin. Build. Environ. 47, 58–66.
Zhang, Z., Zhang, W., Zhai, Z.Q., Chen, Q.Y., 2007. Evaluation of various turbulence models in predicting airflow and turbulence in enclosed environments by CFD: Part-2: comparison with experimental data from literature. HVACR Res. 13 (6), 871–886.
Zhang, Z., Chen, X., Mazumdar, S., Zhang, T., Chen, Q.Y., 2009. Experimental and numerical investigation of airflow and contaminant transport in an airliner cabin mockup. Build. Environ. 44 (1), 85–94.
Zhao, B., Zhang, Y., Li, X., Yang, X., Huang, D., 2004. Comparison of indoor aerosol particle concentration and deposition in different ventilated rooms by numerical method. Build. Environ. 39 (1), 1–8.
Zhou, J., Wei, J.J., Choy, K.T., Sia, S.F., Rowlands, D.K., Yu, D., Wu, C.Y., Lindsley, W.G., Cowling, B.J., McDevitt, J., Peiris, M., Li, Y.G., Yen, H.L., 2018. Defining the sizes of airborne particles that mediate influenza transmission in ferrets. Proc. Natl. Acad. Sci. 115 (10), 2386–2392.